New insights into the catalytic active-site structure of multicopper oxidases

メタデータ	言語: eng
	出版者:
	公開日: 2017-10-03
	キーワード (Ja):
	キーワード (En):
	作成者:
	メールアドレス:
	所属:
URL	http://hdl.handle.net/2297/38226

New insights into the catalytic active-site structure of multicopper oxidases

Hirofumi Komori,[a,b]* Ryosuke Sugiyama,[c] Kunishige Kataoka,[c] Kentaro Miyazaki,[d] Yoshiki Higuchi[b,e] and Takeshi Sakurai[c]*

[a]Faculty of Education, Kagawa University, 1-1 Saiwai-cho, Takamatsu, Kagawa 760-8522, Japan, [b]RIKEN SPring-8 Center, 1-1-1 Koto, Mikazuki-cho, Sayo-gun, Hyogo 679-5198, Japan, [c]Graduate School of Natural Science and Technology, Kanazawa University, Kakuma, Kanazawa 920-1192, Japan, [d]Bioproduction Research Institute, National Institute of Advanced Industrial Science and Technology, Sapporo, Hokkaido 062-8517, Japan, and [e]Graduate School of Life Science, University of Hyogo, 3-2-1 Koto, Kamigori-cho, Ako-gun, Hyogo 678-1297, Japan

Correspondence e-mail:
komori@ed.kagawa-u.ac.jp,
ts0513@kenroku.kanazawa-u.ac.jp

Structural models determined by X-ray crystallography play a central role in understanding the catalytic mechanism of enzymes. However, X-ray radiation generates hydrated electrons that can cause significant damage to the active sites of metalloenzymes. In the present study, crystal structures of the multicopper oxidases (MCOs) CueO from *Escherichia coli* and laccase from a metagenome were determined. Diffraction data were obtained from a single crystal under low to high X-ray dose conditions. At low levels of X-ray exposure, unambiguous electron density for an O atom was observed inside the trinuclear copper centre (TNC) in both MCOs. The gradual reduction of copper by hydrated electrons monitored by measurement of the Cu K-edge X-ray absorption spectra led to the disappearance of the electron density for the O atom. In addition, the size of the copper triangle was enlarged by a two-step shift in the location of the type III coppers owing to reduction. Further, binding of O_2 to the TNC after its full reduction was observed in the case of the laccase. Based on these novel structural findings, the diverse resting structures of the MCOs and their four-electron O_2-reduction process are discussed.

1. Introduction

Structural models determined by X-ray crystallography have played a central role in understanding the catalytic mechanism of a number of enzymes. However, X-ray radiation generates hydrated electrons that can cause significant damage to the active sites of metalloenzymes (O'Neill *et al.*, 2002). In the present study, we determined the crystal structures of the resting multicopper oxidases (MCOs; Kosman, 2010) CueO from *Escherichia coli* (Outten *et al.*, 2001; Roberts *et al.*, 2002) and laccase from a metagenome (mgLAC; Komori *et al.*, 2009a,b), both of which showed characteristic features that led to the proposal of a reaction intermediate under low X-ray dose conditions.

MCOs catalyze the oxidation of a wide range of substrates by reducing O_2 to H_2O without releasing activated oxygen species (Kosman, 2010). Apart from MCOs, only terminal oxidases such as cytochrome *c* oxidase are able to catalyze this process. Thus, MCOs have been proposed to function as cathodic enzymes for biofuel cells. MCOs are comprised of structural units of cupredoxin-like domains and are classified into the following three groups according to the number of domains: the two-domain type (2dMCOs), the three-domain type (3dMCOs) and the six-domain type (6dMCOs) (Komori & Higuchi, 2010). These enzymes share similar spectroscopic properties related to the copper ions in the active site. MCOs contain three different types of copper ions, all of which are

Table 1
Summary of crystallographic data for CueO.

Values in parentheses are for the highest resolution shell. All data (from data 1 to data 7) were collected from the same crystal (of dimensions $0.1 \times 0.2 \times 0.6$ mm).

	Data 1†	Data 2	Data 3	Data 4	Data 5‡	Data 6	Data 7
Source	SPring-8, BL26B2 ($\sim 10^{11}$ photons s^{-1}, beam size 150×150 µm)						
Wavelength (Å)	0.8000	0.8000	1.3700	0.8000	0.8000	0.8000	1.3700
Aluminium attenuator (µm)	1000						
Exposure time (s)	~ 7§	180	180	180	1800	180	180
Resolution (Å)	50.00–1.60	50.00–1.30	50.00–1.70	50.00–1.30	50.00–1.06	50.00–1.30	50.00–1.70
No. of unique reflections	59209	113899	51458	113631	209935	112228	51156
Multiplicity	3.6 (2.4)	3.8 (3.2)	3.6 (3.6)	3.7 (3.0)	4.4 (3.2)	3.7 (2.6)	3.5 (3.5)
Completeness (%)	96.0 (72.6)	99.5 (95.6)	99.8 (99.0)	99.2 (92.8)	99.4 (94.8)	97.9 (81.9)	99.1 (98.9)
$\langle I/\sigma(I)\rangle$	18.4 (2.7)	26.3 (2.9)	36.2 (9.7)	26.2 (2.7)	33.8 (2.5)	24.8 (2.0)	34.3 (8.1)
R_{merge}¶	0.061 (0.235)	0.045 (0.309)	0.041 (0.119)	0.044 (0.315)	0.047 (0.377)	0.045 (0.373)	0.041 (0.139)
Refinement statistics							
R/R_{free}††	0.168/0.211	0.137/0.178		0.137/0.179	0.127/0.156	0.138/0.182	
R.m.s.d. (Å)							
Bond lengths	0.008	0.011		0.011	0.015	0.011	
Bond angles	0.025	0.029		0.029	0.033	0.029	
Occupancy of type III copper							
T3Cu$_a$ (oxidized/reduced)	0.90/0.00	0.68/0.22		0.35/0.55	0.28/0.62	0.00/0.90	
T3Cu$_b$ (oxidized/reduced)	0.90/0.00	0.90/0.00		0.47/0.43	0.38/0.52	0.00/0.90	
No. of residues	476	476		476	476	476	
No. of waters	429	482		482	522	481	
No. of copper ions	4	4		4	4	4	
Average B factors (Å^2)							
Protein	17.2	16.7		16.9	15.6	17.7	
Waters	28.3	28.8		28.8	29.4	30.6	
Copper ions	10.6	9.8		9.5	8.9	11.4	
Acetate ions		16.0		16.5	16.5	17.6	
PDB entry	4ner	4e9q		4e9r	4e9s	4e9t	

† The crystal was translated three times during data collection in order to reduce the X-ray exposure. ‡ A high-resolution data det (data 5) and a low-resolution data set (data 4) were merged. § An aluminium attenuator (1000 µm) was used in order to reduce the X-ray intensity by one seventh at 0.8000 Å. ¶ $R_{merge} = \sum_{hkl} \sum_i |I_i(hkl) - \langle I(hkl)\rangle| / \sum_{hkl} \sum_i I_i(hkl)$. †† $R = \sum_{hkl} ||F_{obs}| - |F_{calc}|| / \sum_{hkl} |F_{obs}|$. R_{free} is the cross-validation R factor computed for a test set of 5% of the unique reflections.

involved in the transfer of electrons from the substrate to O_2, the final electron acceptor. The type I copper (T1Cu) mediates electron transfer between the substrate and the trinuclear copper centre (TNC). The key element for O_2 reduction is the TNC, comprised of one type II (T2Cu) and a pair of type III (T3Cu) copper ions, in which the final electron acceptor O_2 is bound and reduced to two water molecules (Bento *et al.*, 2005; Sakurai & Kataoka, 2007; Solomon *et al.*, 2008). A variety of X-ray crystal structures have been reported for the TNC in resting MCOs (Messerschmidt *et al.*, 1989; Hakulinen *et al.*, 2002; Roberts *et al.*, 2002; Enguita *et al.*, 2003; Taylor *et al.*, 2005). These structures contain the following common TNC features: the T2Cu is coordinated by two histidines and an OH$^-$ or H_2O and the two T3Cus are each coordinated by three histidines and have a bridged OH$^-$ between them. Therefore, the T2Cu is magnetically isolated, affording an electron paramagnetic resonance (EPR) signal typical of tetragonal copper with a large $A_\parallel$ value. In contrast, the T3Cus are not detected by EPR owing to strong antiferromagnetic coupling through the bridged OH$^-$ ion.

The four-electron O_2-reduction mechanism of MCOs has been proposed to function through two reaction intermediates: intermediate I (the peroxide intermediate) and intermediate II (the native intermediate). O_2^{2-} has been proposed to be bound between the T3Cus in intermediate I. However, no direct evidence to show the binding of peroxide at the TNC, in which T2Cu is cuprous and the T3Cus are cupric, has been obtained. Although we have crystallized the

Cys500Ser/Glu506Gln double mutant of CueO for determination of the structure of the peroxide-binding form, the TNC changed to afford the O-inside structure, which had been supposed for intermediate II, even under low-dose X-ray radiation conditions (Komori *et al.*, 2012). Intermediate II has been considered to be a four-electron reduced form as for O_2 (Huang *et al.*, 1999; Kataoka *et al.*, 2009). One of the O atoms derived from O_2 is bridged between the T3Cus as OH$^-$, while the other is located in the inside of the TNC as O^{2-} or OH$^-$, affording a broad EPR signal with $g < 2$ which was only detectable at cryogenic temperatures because the three Cu centres in the TNC are strongly magnetically coupled. On the other hand, it has recently been proposed that the T3Cus and a tyrosine radical are magnetically coupled from a kinetic study on a 2dMCO, SLAC (Tepper *et al.*, 2009), although the tyrosine residue is not conserved in the corresponding position near the TNC in the 3dMCOs. With the decay of intermediate II, the $g < 2$ EPR signal disappears and the T2Cu EPR signal is detected, reaching the resting form *via* steps in which the central O atom is converted into a water molecule by accepting protons supplied through a hydrogen-bond network constructed from an acidic amino acid and water molecules (Komori *et al.*, 2013). Since the central O atom in the TNC is not present in the resulting resting form, the question arises as to why the T-shaped three-coordinated T2Cu centre is only paramagnetic in the TNC in MCOs.

All of the copper centres in MCOs have high redox potentials and are very sensitive to the X-ray radiation used in

crystal structure analyses. The reported structures determined by X-ray crystallography may possibly represent mixtures of different stages of the catalytic reactions (Hakulinen *et al.*, 2006; Ferraroni *et al.*, 2007, 2012; Polyakov *et al.*, 2009; De la Mora *et al.*, 2012). Therefore, it is difficult to distinguish the structures of the active sites associated with each redox state. In this study, we performed X-ray crystal structure analyses of the resting forms of a 3dMCO (CueO) and a 2dMCO (mgLAC) using low to high doses of X-ray radiation.

2. Materials and methods

The protein purification and crystallization of CueO and mgLAC were performed according to previously reported methods (Kataoka *et al.*, 2007; Komori *et al.*, 2009a). For data collection, CueO crystals were soaked in a cryoprotectant

solution (10% glycerol) for a few minutes prior to cooling under a cold stream of nitrogen, whereas mgLAC crystals were directly cooled under a cold stream of nitrogen. X-ray diffraction data sets were collected at 100 K on beamline BL26B2 ($\lambda = 0.8000$ and 1.3700 A) at SPring-8 using a MAR Research MX225 CCD detector (Ueno *et al.*, 2006). In addition, K-edge X-ray absorption spectra (XAS) of copper ions were collected using a Si PIN photodiode detector and a multichannel analyzer. The unit-cell parameters were determined and the reflections were integrated using *HKL*-2000 (Otwinowski & Minor, 1997) and the *CCP*4 program package (Winn *et al.*, 2011). Using the reported structures of CueO (PDB entry 1kv7; Roberts *et al.*, 2002) and mgLAC (PDB entry 2zwn; Komori *et al.*, 2009b), the molecular-replacement method was carried out. Further model building and structure refinement was performed using *Coot* (Emsley & Cowtan, 2004), *REFMAC* (Murshudov *et al.*, 2011) and *SHELX* (Sheldrick, 2008). Individual anisotropic B-factor refinement was carried out with DELU and SIMU restaints. The ratio of oxidized and reduced T3Cus was determined by occupancy refinement with *SHELX*. The progress and validity of the refinement process were checked by monitoring the R_{free} value calculated using 5% of the total reflections (Brünger, 1992). Data-collection and refinement statistics are summarized in Tables 1 and 2. Model geometry was analyzed using *MolProbity* (Chen *et al.*, 2010) and no residues were found in the disallowed region of the Ramachandran plot. The figures were prepared using *PyMOL* (http://www.pymol.org). Coordinates have been deposited in the PDB with accession codes 4ner, 4e9q, 4e9r, 4e9s, 4e9t, 4e9v, 4e9w, 4e9x and 4e9y.

3. Results and discussion

Diffraction data were collected at different X-ray exposure times from single crystals of CueO and mgLAC (Tables 1 and 2). Fig. 1 shows the TNC structure of CueO in its resting form obtained from the lowest to higher X-ray exposure conditions. The TNC structure at the lowest X-ray exposure (data 1 in Figs. 1a and 1b) is completely different from the previously reported struc-
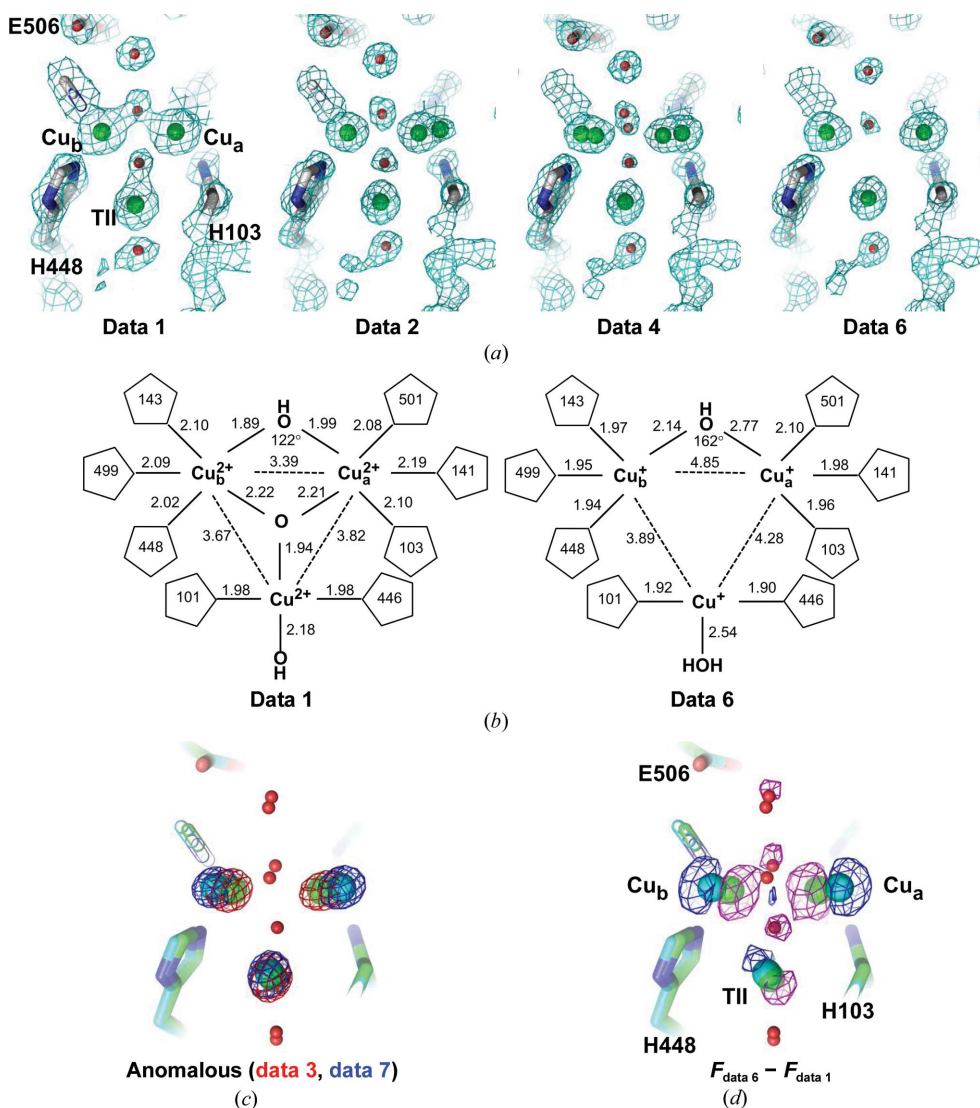

Figure 1
Structure of the TNC of CueO. (a) $2F_o - F_c$ maps (contoured at 1.2σ) for data 1, 2, 4 and 6 (Cu and O are shown as green and red spheres, respectively). (b) Bond distances and the bond angle T3Cu$_b$—OH—T3Cu$_b$ for data 1 and 6. The three Cu and O atoms are essentially coplanar. (c) Anomalous map (contoured at 20σ) for data 3 (red) and 7 (blue). (d) $F_o - F_o$ maps (contoured at 10σ) for data 1 − data 6 (red) and for data 6 − data 1 (blue).

Table 2
Summary of the crystallographic data for mgLAC.

Values in parentheses are for the highest resolution shell. All data (from data 1 to data 4) were collected from the same crystal (of dimensions $0.05 \times 0.2 \times 0.3$ mm).

	Data 1	XAS 1	Data 2	XAS 2	Data 3	XAS 3	Data 4	XAS 4
Source	SPring-8, BL26B2 ($\sim 10^{11}$ photons s^{-1}, beam size 150×150 μm)							
Wavelength (Å)	0.8000	1.3770–1.3820	0.8000	1.3770–1.3820	0.8000	1.3770–1.3820	0.8000	1.3770–1.3820
Aluminium attenuator (μm)	600	200	600	200		200		200
Exposure time (s)	~ 26†	~ 8‡	180	~ 8‡	1800	~ 8‡	180	~ 8‡
Resolution (Å)	50.00–1.80		50.00–1.45		50.00–1.14		50.00–1.50	
No. of unique reflections	87564		166428		209935		149764	
Multiplicity	7.5 (7.4)		7.4 (6.9)		7.1 (5.3)		7.1 (4.6)	
Completeness (%)	99.9 (100.0)		99.9 (100.0)		99.0 (93.2)		99.3 (95.2)	
$\langle I/\sigma(I)\rangle$	16.9 (3.8)		19.0 (2.3)		28.2 (2.3)		19.6 (2.2)	
R_{merge}§	0.105 (0.385)		0.093 (0.623)		0.064 (0.507)		0.086 (0.462)	
Refinement statistics								
R/R_{free}¶	0.163/0.215		0.141/0.194		0.141/0.172		0.171/0.208	
R.m.s.d. (Å)								
Bond lengths	0.006		0.009		0.014		0.009	
Bond angles	0.023		0.027		0.031		0.026	
No. of residues	949		949		949		1754	
No. of waters	753		851		867		949	
No. of copper ions	4		4		4		4	
Average B factors (Å^2)								
Protein	13.0		13.6		13.2		13.7	
Water	23.9		26.3		25.1		25.9	
Copper ions	15.2		14.8		11.9		13.0	
PDB entry	4e9v		4e9w		4e9x		4e9y	

† A 600 μm aluminium attenuator was used in order to reduce the X-ray intensity by one seventh at 0.8000 Å. ‡ A 200 μm aluminium attenuator was used in order to reduce the X-ray intensity by one seventh at 1.38 Å. § $R_{\text{merge}} = \sum_{hkl} \sum_i |I_i(hkl) - \langle I(hkl)\rangle| / \sum_{hkl} \sum_i I_i(hkl)$. ¶ $R = \sum_{hkl} ||F_{\text{obs}}| - |F_{\text{calc}}|| / \sum_{hkl} |F_{\text{obs}}|$. R_{free} is the cross-validation R factor computed for a test set of 5% of the unique reflections.

tures of resting CueO (Roberts *et al.*, 2002) and the deletion mutant (Kataoka *et al.*, 2007). In addition to an OH⁻ bridged between the T3Cus, an unambiguous electron density (O atom) was observed inside the TNC, as has been proposed for intermediate II (Komori *et al.*, 2012). The Cu—Cu distances indicate that an isosceles copper triangle is formed with longer T2Cu—T3Cu distances of 3.7 and 3.8 Å and a shorter T3Cu—T3Cu distance of 3.4 Å. The distances between the central O atom and the three copper centres are 1.94, 2.21 and 2.22 Å, indicating that the O atom is not located in the middle of the triangle but is slightly nearer to T2Cu.

Cu K-edge spectra were measured in order to monitor changes in the redox states of the copper centres derived from the hydrated electrons formed by synchrotron radiation. Soon after the first X-ray exposure for 7 s, all copper ions were in the cupric state, as shown by the Cu K-edge X-ray absorption spectra (Fig. 2). Reduction of copper atoms gradually took place upon the X-ray exposure of a single crystal of CueO, as shown in Fig. 2, producing an $1s \rightarrow 4p_z$, ~ 8984 eV feature. An anomalous Fourier map (data 3 and data 7) clearly shows two different positions of T3Cus with varying X-ray exposure times (Fig. 1c). The size of the copper triangle was enlarged in a two-step shift with the reduction of copper ions (Fig. 1). During the X-ray exposure, T3Cu$_a$ shifted towards His103 and His141 and T3Cu$_b$ shifted towards the three His ligands in a slower process, resulting in a T3Cu—T3Cu distance of 4.9 Å. Simultaneously, the T3Cu—OH⁻—T3Cu angle changed from 122 to 162° and the O atom inside the copper triangle disappeared (Figs. 1a and 1b). In addition, the difference Fourier map between data 1 and data 6 indicated that a change

occurred in the T2Cu (Fig. 1d). The bond length between T2Cu and the O atom (outside) changed from 2.2 to 2.5 Å, which is possibly owing to the protonation of OH⁻ to give H$_2$O coupled with the reduction of T2Cu. On high X-ray exposure (data 6), we observed a structure in which almost all of the coppers in the TNC were reduced, although T3Cu$_b$ was still partly in the cupric form with the binding of a hydroxide ion. If we continued X-ray irradiation further, CueO would have reached the fully reduced form and the second water
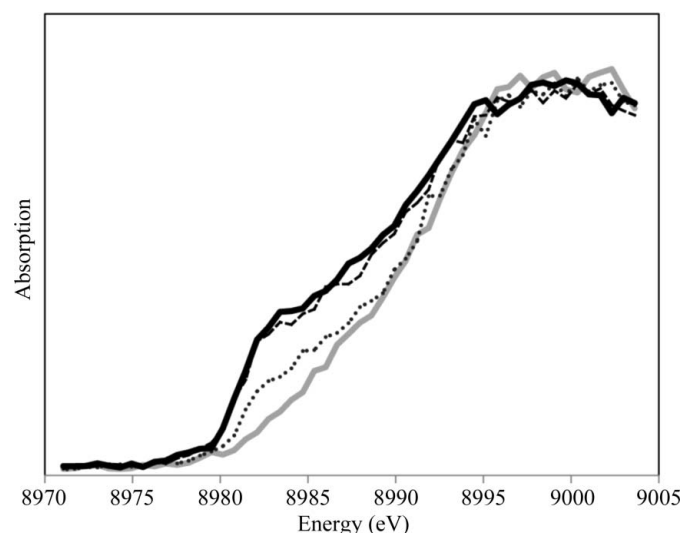
Figure 2
Cu K-edge X-ray absorption spectra of CueO. The X-ray absorption spectrum of CueO is shown after X-ray exposures of 7, 187, 18 187 and 18 367 s (grey, dotted, dashed and black lines, respectively).
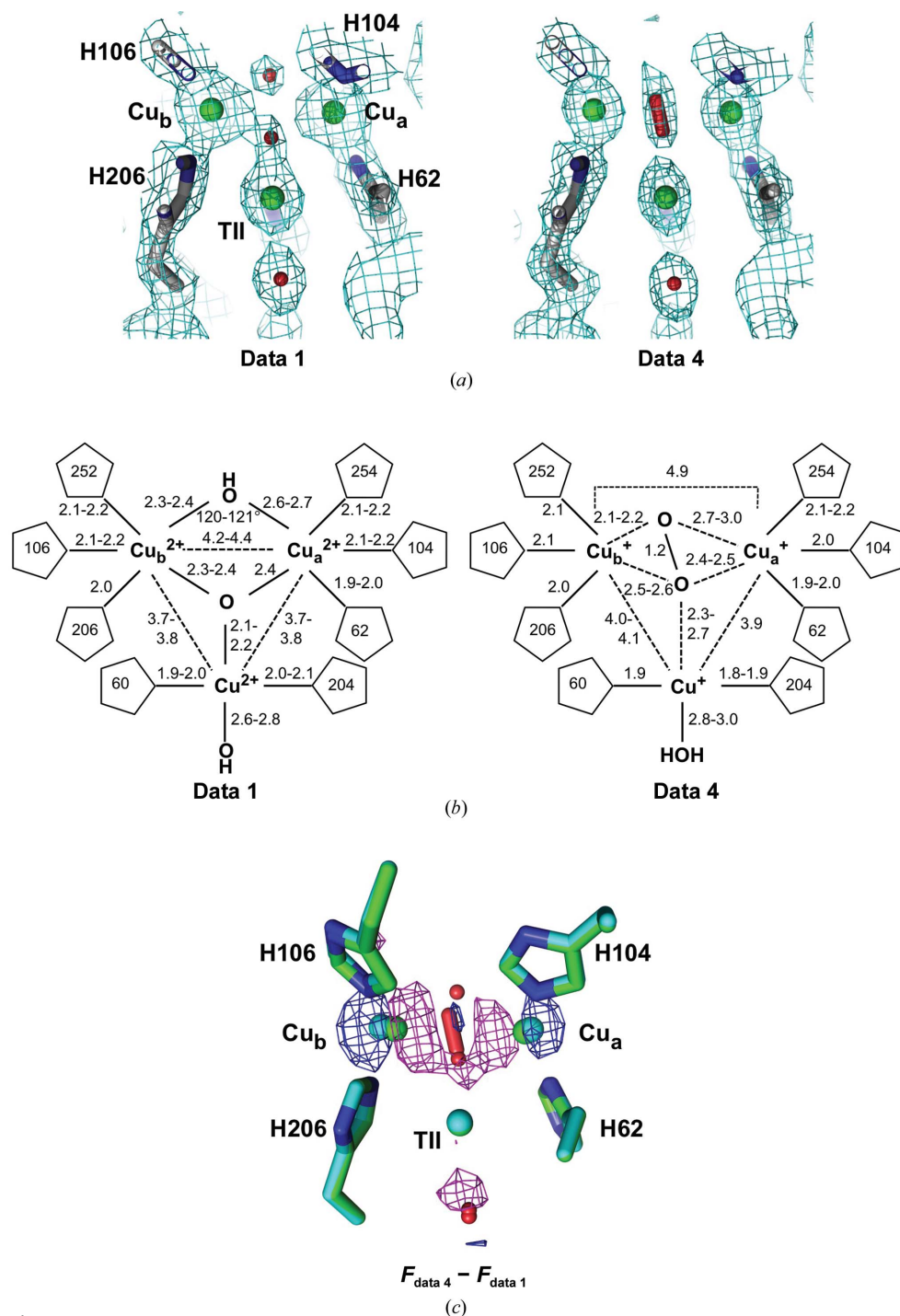
Figure 3
Structure of the TNC of mgLAC. (*a*) $2F_o - F_c$ maps (contoured at 1.2σ) for data 1 and 4 (Cu and O atoms are shown as green and red spheres, respectively). (*b*) Bond distances and the bond angle T3Cu$_a$—OH—T3Cu$_b$ for data 1 and 4. (*c*) $F_o - F_o$ maps (contoured at 6σ) for data 1 − data 4 (red) and for data 4 − data 1 (blue).

though the classical resting form in which all copper centres in the TNC are cupric and T3Cus are bridged with OH⁻ because the O atom (inside) is eliminated as H_2O coupled with reduction of the TNC.

We observed the same characteristic features for the TNC of mgLAC. At low X-ray exposure (data 1), mgLAC also contains an O-inside TNC, although the copper centres in the TNC appear to be partly reduced according to the feature measured at approximately 8984 eV in the X-ray absorption spectra (XAS) after collecting diffraction data 1. Similarly to CueO, changes in the size of the copper triangle and the bond length between T2Cu and the O atom (outside) were observed after exposure of the mgLAC crystal to X-rays for long times (Figs. 3 and 4). At high X-ray exposure (data 4) after the full reduction of the copper centres, mgLAC showed an elongated density between the T3Cus. This density is considered to represent the binding of dioxygen to a reduced form of mgLAC, as has also been identified in other MCOs (Hakulinen *et al.*, 2006; Ferraroni *et al.*, 2007). The binding mode of dioxygen between the T3Cus is in a μ-1,2-peroxo-like fashion, as has been proposed for intermediate 1 (the peroxide intermediate; Solomon *et al.*, 2008; Kataoka *et al.*, 2009). The resolution for data 4 was not sufficiently high to discuss the bond length between the O atoms (1.5 Å), but the present results unequivocally show that mgLAC reached intermediate I after passing through the fully reduced form and reacting with dioxygen, in contrast to CueO.

molecule might have been eliminated from the TNC. Thus, the changes observed from data 1 to data 6 indicate that the water molecules are formed with the stepwise reduction of the copper centres, *i.e.* in steps from a fully oxidized resting form with the O atoms (inside and outside) but with no water yet formed to the fully reduced form for the next enzymatic cycle. Under steady-state conditions, however, CueO may not pass

T1Cu in CueO and mgLAC was also gradually reduced by hydrated electrons, as shown by the colour changes of the crystal (from a blue colour to almost colourless) during X-ray irradiation (Figs. 5 and 6 and Supplementary Fig. S1[1]).

Although full reduction of T1Cu did not take place owing to its more negative redox potential compared with those of T2Cu and the T3Cus, electrons were transferred from T1Cu to the TNC through the His–Cys–His pathway until a thermo-dynamic equilibrium state was reached. The reduction of T1Cu slightly moves the ion away from the methionine axial ligand down to a trigonal plane composed of two histidines and a cysteine. The T1Cu–ligand bond distances were also observed to decrease by sub-angstrom distances ($\sim$0.1 Å) on reduction. On the other hand, the bond length between T2Cu and the exogenous O atom located outside the TNC triangle in mgLAC was considerably lengthened compared with that in CueO, 2.6–2.8 Å in data 1 and 2.8–3.0 Å in data 4, indicating that the water molecule is kept bound to T2Cu regardless of its oxidation state (Fig. 3b), in contrast to CueO (Fig. 1b). This apparent difference between CueO and mgLAC would derive from the difference in the Lewis acid character of T2Cu.

Our X-ray crystallographic data obtained at low X-ray exposure conditions for both CueO and mgLAC exhibited the O-inside TNC structure, in contrast to the classical TNC structure without an O (inside) atom reported previously for many resting MCOs including CueO (Messerschmidt et al., 1989; Hakulinen et al., 2002; Roberts et al., 2002; Enguita et al., 2003; Taylor et al., 2005). The O-inside TNC structure has been observed as a minor form in resting laccases (Polyakov et al., 2009), and it is now accepted that the classical resting form without the O (inside) atom might not be the exclusive form for resting MCOs, although the diffraction data for all MCOs were not necessarily obtained under low X-ray exposure conditions.

The O-inside TNC structure was supposed to be a unique structure of intermediate II (the native intermediate), which can be trapped by mutating a Glu residue located in the proton-relay pathway. Intermediate II gives a broad $g < 2$ EPR signal at cryogenic temperatures and absorption bands at $\sim$350 and $\sim$400 nm (shoulder), both of which originate from the magnetically coupled structures of the TNC. With the decay of intermediate II, the EPR signal of T2Cu becomes detectable since T2Cu is magnetically isolated owing to the elimination of the O (inside) atom from the TNC as a water molecule. Therefore, it has been considered that the magnetic interaction between the copper centres can be attributed to the O atom located inside the TNC together with the O (outside) atom bridged between the T3Cus. In contrast to these results obtained from 3dMCOs, a contribution from a Tyr radical has been proposed for the 2dMCO SLAC (Tepper et al., 2009). Tyr108 at a distance of $\sim$4.6 Å from an imidazole group coordinated to T2Cu has been considered to function as the fourth electron donor to O_2 in analogy to the O_2-reduction mechanism by terminal oxidases with a cross-linked Tyr (Mochizuki et al., 1999). However, the tyrosyl residue is not conserved in the corresponding position in the 3dMCO CueO, and mutations at Tyr69 and Tyr496 at a distance of >5.7 Å from the His imidazole ligand of the T3Cus did not suggest the involvement of these Tyr residues in dioxygen reduction (T. Kajikawa, M. Yamamoto, K. Kataoka & T. Sakurai, unpub-lished data). The indole ring of Trp139 is stacked on the

imidazole ring of His103 coordinated to one of the T3Cus. However, a preliminary mutation of this Trp residue also excluded this amino acid as a source of electrons. The present results unequivocally show that the resting CueO contains the O (inside) atom in the TNC. However, the resting CueO does not give the $g < 2$ EPR signal detected for intermediate II but gives the T2Cu EPR signal. Therefore, we may need to obtain more detailed structural information about the bond length and bond angle of the resting CueO and mgLAC to explain the difference in magnetic properties originating in the O (inside) structure of the TNC, including possible protonation of the O-inside atom in the resting form.

Recently, we performed crystal structure analyses of the Cys500Ser/Glu506Gln CueO mutant with the aim of revealing the structure of intermediate I (the peroxide intermediate). However, its facile conversion to the O-inside TNC structure took place even under low X-ray exposure conditions. The size of the O-inside TNC was slightly smaller compared with the resting CueO: the Cu—Cu distances were 3.22, 3.61 and 3 65 Å and the Cu—O (inside) distances were 1.83, 2.08 and 2.26 Å (Komori et al., 2012). It is not known whether this structure with a smaller sized copper triangle and shorter bond distances accounts for the strong magnetic interactions between the three copper centres in intermediate II and the magnetic isolation of T2Cu in the resting CueO, although it is also unknown whether or not a proton is attached to the O (inside) atom in the resting TNC structure. Recently, it has been reported that T2Cu in the resting MCO is not completely isolated magnetically (Zaballa et al., 2010).

If an MCO with the O-inside TNC structure gradually loses the O (inside) atom as H_2O and reaches another stable state, it is not conflicting that MCOs may have two resting forms with and without the O atom inside the TNC. CueO and mgLAC might favour the O-inside TNC form, but the prototype MCO ascorbate oxidase and many others may
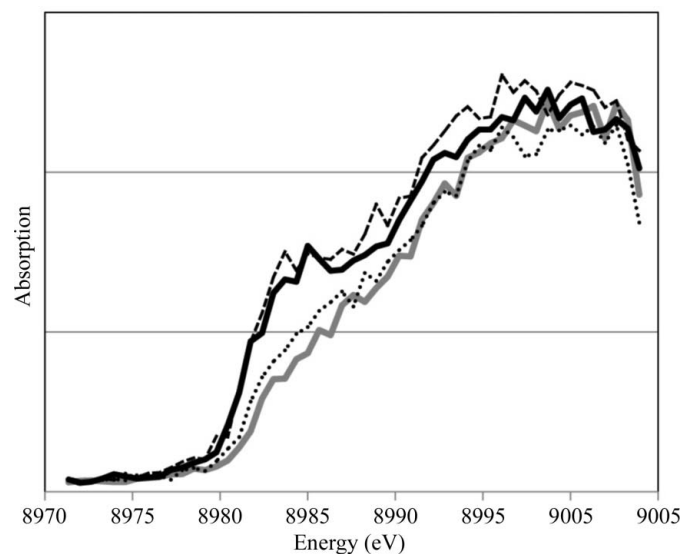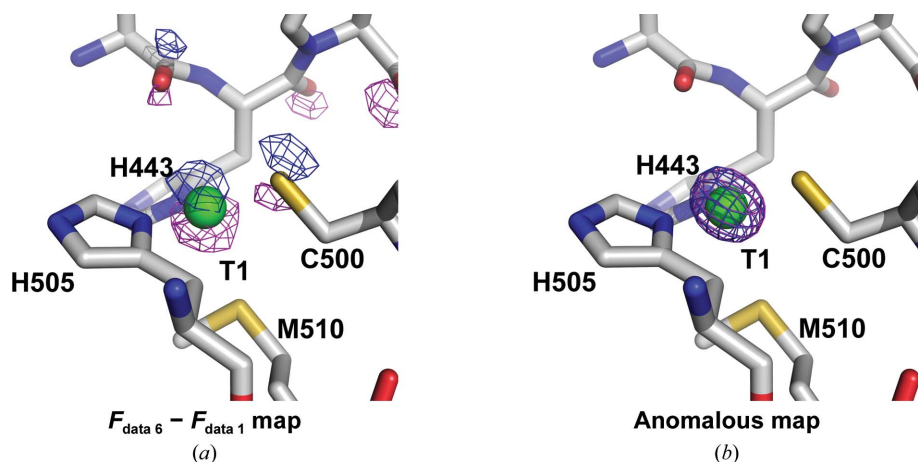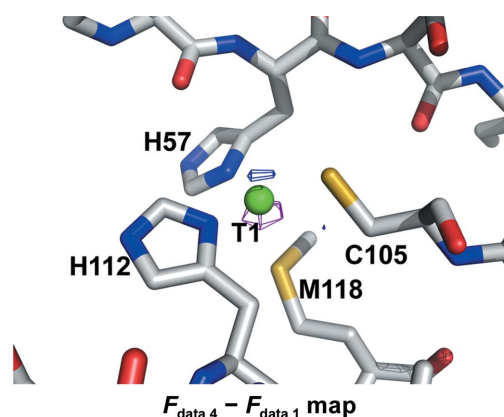

Figure 4
Cu K-edge X-ray absorption spectra of mgLAC (Table 2). XAS 1, XAS 2, XAS 3 and XAS 4 are shown as grey, dotted, dashed and black lines, respectively.

Figure 5
T1Cu site of CueO. (a) $F_o - F_o$ maps (contoured at 10σ) for data 1 − data 6 (red) and for data 6 − data 1 (blue). (b) Anomalous maps (20σ) for data 3 (red) and data 7 (blue).

Figure 6
T1Cu site of mgLAC. $F_o - F_o$ maps (6σ) for data 1 − data 4 (red) and for data set 4 − data set 1 (blue).

We obtained analogous results with independently prepared CueO using the same crystallization conditions and using crystallization conditions with different pH and buffer solutions. Therefore, the present results are not accidental, and resting CueO and mgLAC prefer the O-inside TNC structure in the resting form, although it remains unclear whether this state is intermediate II (the native intermediate) itself or a form with the O-inside TNC subsequent to intermediate II. To examine the latter case, the structure of the TNC in the intermediate II and its decay need to be studied in more detail. In addition, re-examination of previously structurally determined MCOs and careful X-ray crystal structure analyses of novel MCOs need to be performed in order to determine whether the O-inside TNC structure prevails widely as the resting form over many MCOs or whether it is limited to CueO and mgLAC.

favour the classical resting form. Although additional studies are required, our data indicate that the electron density of the O (inside) atom does decrease with reduction of the copper centres in the TNC, in which T2Cu is most readily reduced and is followed by the reduction of T3Cu$_a$ and finally the reduction of T3Cu$_b$. Previous studies on Fet3p, a 3dMCO (Augustine *et al.*, 2010), and the Cys500Ser/Glu506Gln mutant of CueO (Komori *et al.*, 2012) showed that the two T3Cus are structurally asymmetric, and this heterogeneity of the two T3Cus was also observed in the reduction steps to form water molecules. The present data also support the asymmetry of the T3Cus in the reduction process. The different redox distributions of the T3Cus will be owing to the negatively charged residue (Asp112) located in the second coordination sphere around T3Cu$_b$ and Trp139 near the His103 coordinated to T3Cu$_a$. This characteristic asymmetry functionally contributes to the formation of water molecules, and these structural features will be common at least to 3dMCOs, while the preferred resting form is diverse and/or becomes complicated owing to the facile reduction of the copper centres during X-ray crystal structure analyses.

References

Augustine, A. J., Kjaergaard, C., Qayyum, M., Ziegler, L., Kosman, D. J., Hodgson, K. O., Hedman, B. & Solomon, E. I. (2010). *J. Am. Chem. Soc.* **132**, 6057–6067.

Bento, I., Martins, L. O., Lopes, G. G., Carrondo, M. A. & Lindley, P. F. (2005). *Dalton Trans.*, pp. 3507–3513.

Brünger, A. T. (1992). *Nature (London)*, **355**, 472–475.

Chen, V. B., Arendall, W. B., Headd, J. J., Keedy, D. A., Immormino, R. M., Kapral, G. J., Murray, L. W., Richardson, J. S. & Richardson, D. C. (2010). *Acta Cryst.* D**66**, 12–21.

De la Mora, E., Lovett, J. E., Blanford, C. F., Garman, E. F., Valderrama, B. & Rudino-Pinera, E. (2012). *Acta Cryst.* D**68**, 564–577.

Emsley, P. & Cowtan, K. (2004). *Acta Cryst.* D**60**, 2126–2132.

Enguita, F. J., Martins, L. O., Henriques, A. O. & Carrondo, M. A. (2003). *J. Biol. Chem.* **278**, 19416–19425.

Ferraroni, M., Matera, I., Chernykh, A., Kolomytseva, M., Golovleva, L. A., Scozzafava, A. & Briganti, F. (2012). *J. Inorg. Biochem.* **111**, 203–209.

Ferraroni, M., Myasoedova, N. M., Schmatchenko, V., Leontievsky, A. A., Golovleva, L. A., Scozzafava, A. & Briganti, F. (2007). *BMC Struct. Biol.* **7**, 60.

Hakulinen, N., Kiiskinen, L. L., Kruus, K., Saloheimo, M., Paananen, A., Koivula, A. & Rouvinen, J. (2002). *Nature Struct. Biol.* **9**, 601–605.

Hakulinen, N., Kruus, K., Koivula, A. & Rouvinen, J. (2006). *Biochem. Biophys. Res. Commun.* **350**, 929–934.

Huang, H., Zoppellaro, G. & Sakurai, T. (1999). *J. Biol. Chem.* **274**, 32718–32724.

Kataoka, K., Komori, H., Ueki, Y., Konno, Y., Kamitaka, Y., Kurose, S., Tsujimura, S., Higuchi, Y., Kano, K., Seo, D. & Sakurai, T. (2007). *J. Mol. Biol.* **373**, 141–152.

Kataoka, K., Sugiyama, R., Hirota, S., Inoue, M., Urata, K., Minagawa, Y., Seo, D. & Sakurai, T. (2009). *J. Biol. Chem.* **284**, 14405–14413.

Komori, H. & Higuchi, Y. (2010). *Biomol. Concepts*, **1**, 31–40.

Komori, H., Kajikawa, T., Kataoka, K., Higuchi, Y. & Sakurai, T. (2013). *Biochem. Biophys. Res. Commun.* **438**, 686–690.

Komori, H., Miyazaki, K. & Higuchi, Y. (2009*a*). *Acta Cryst.* F**65**, 264–266.

Komori, H., Miyazaki, K. & Higuchi, Y. (2009*b*). *FEBS Lett.* **583**, 1189–1195.

Komori, H., Sugiyama, R., Kataoka, K., Higuchi, Y. & Sakurai, T. (2012). *Angew. Chem. Int. Ed.* **51**, 1861–1864.

Kosman, D. J. (2010). *J. Biol. Inorg. Chem.* **15**, 15–28.

Messerschmidt, A., Rossi, A., Ladenstein, R., Huber, R., Bolognesi, M., Gatti, G., Marchesini, A., Petruzzelli, R. & Finazzi-Agró, A. (1989). *J. Mol. Biol.* **206**, 513–529.

Mochizuki, M., Aoyama, H., Shinzawa-Itoh, K., Usui, T., Tsukihara, T. & Yoshikawa, S. (1999). *J. Biol. Chem.* **274**, 33403–33411.

Murshudov, G. N., Skubák, P., Lebedev, A. A., Pannu, N. S., Steiner, R. A., Nicholls, R. A., Winn, M. D., Long, F. & Vagin, A. A. (2011). *Acta Cryst.* D**67**, 355–367.

O'Neill, P., Stevens, D. L. & Garman, E. (2002). *J. Synchrotron Rad.* **9**, 329–332.

Otwinowski, Z. & Minor, W. (1997). *Methods Enzymol.* **276**, 307–326.

Outten, F. W., Huffman, D. L., Hale, J. A. & O'Halloran, T. V. (2001). *J. Biol. Chem.* **276**, 30670–30677.

Polyakov, K. M., Fedorova, T. V., Stepanova, E. V., Cherkashin, E. A., Kurzeev, S. A., Strokopytov, B. V., Lamzin, V. S. & Koroleva, O. V. (2009). *Acta Cryst.* D**65**, 611–617.

Roberts, S. A., Weichsel, A., Grass, G., Thakali, K., Hazzard, J. T., Tollin, G., Rensing, C. & Montfort, W. R. (2002). *Proc. Natl Acad. Sci. USA*, **99**, 2766–2771.

Sakurai, T. & Kataoka, K. (2007). *Cell. Mol. Life Sci.* **64**, 2642–2656.

Sheldrick, G. M. (2008). *Acta Cryst.* A**64**, 112–122.

Solomon, E. I., Augustine, A. J. & Yoon, J. (2008). *Dalton Trans.*, pp. 3921–3932.

Taylor, A. B., Stoj, C. S., Ziegler, L., Kosman, D. J. & Hart, P. J. (2005). *Proc. Natl Acad. Sci. USA*, **102**, 15459–15464.

Tepper, A. W., Milikisyants, S., Sottini, S., Vijgenboom, E., Groenen, E. J. & Canters, G. W. (2009). *J. Am. Chem. Soc.* **131**, 11680–11682.

Ueno, G., Kanda, H., Hirose, R., Ida, K., Kumasaka, T. & Yamamoto, M. (2006). *J. Struct. Funct. Genomics*, **7**, 15–22.

Winn, M. D. *et al.* (2011). *Acta Cryst.* D**67**, 235–242.

Zaballa, M. E., Ziegler, L., Kosman, D. J. & Vila, A. J. (2010). *J. Am. Chem. Soc.* **132**, 11191–11196.